Published on 22 March 2016. Downloaded by Korea Institute of Science and Technology / KIST on 29/07/2016 02:26:52.

PCCP

PAPER

View Article Online
View Journal | View Issue

Cite this: *Phys. Chem. Chem. Phys.*, 2016, **18**, 11073

Isolation of pristine MXene from Nb_4AlC_3 MAX phase: a first-principles study†

Avanish Mishra,‡[a] Pooja Srivastava,‡[a] Hiroshi Mizuseki,[b] Kwang-Ryeol Lee[b] and Abhishek K. Singh*[a]

Received 9th December 2015,
Accepted 22nd March 2016

DOI: 10.1039/c5cp07609a

www.rsc.org/pccp

Synthesis of pristine MXene sheets from MAX phase is one of the foremost challenges in getting a complete understanding of the properties of this new technologically important 2D-material. Efforts to exfoliate Nb_4AlC_3 MAX phase always lead to Nb_4C_3 MXene sheets, which are functionalized and have several Al atoms attached. Using the first-principles calculations, we perform an intensive study on the chemical transformation of MAX phase into MXene sheets by inserting HF, alkali atoms and LiF in Nb_4AlC_3 MAX phase. Calculated bond-dissociation energy (BDE) shows that the presence of HF in MAX phase always results in functionalized MXene, as the binding of H with MXene is quite strong while that with F is weak. Insertion of alkali atoms does not facilitate pristine MXene isolation due to the presence of chemical bonds of almost equal strength. In contrast, weak Li–MXene and strong Li–F bonding in Nb_4AlC_3 with LiF ensured strong anisotropy in BDE, which will result in the dissociation of the Li–MXene bond. *Ab initio* molecular dynamics calculations capture these features and show that at 500–650 K, the Li–MXene bond indeed breaks leaving a pristine MXene sheet behind. The approach and insights developed here for chemical exfoliation of layered materials bonded by chemical bonds instead of van der Waals can promote their experimental realization.

Introduction

Successful isolation of graphene[1] and subsequent discovery of its extraordinary properties stimulated extensive research into the synthesis and characterization of new 2D-materials. In this search, many 2D-materials, *e.g.*, hexagonal boron-nitride (h-BN),[2] transition-metal dichalcogenides (TMDs),[3] phosphorene,[4] *etc.* have been synthesized and their usage in a range of applications has been demonstrated. Recently, 2D layers of early transition metal carbides and/or nitrides, called MXene,[5,6] have been synthesized from the MAX phase[5,7] ($M_{n+1}AX_n$, M = early transition metal, A = group IIIA or IVA element and X = carbon and/or nitrogen) by removing the A element using aqueous hydrofluoric acid.[5,8] Contrary to van der Waals solids, in MAX, the MXene layers are bonded with strong metallic bonds between M and A atoms.[9] Similar to its parent material MAX, MXene possesses a combination of metallic[10–14] and ceramic properties,[9] *e.g.*, high melting point, low electrical resistivity, high corrosion resistance and hardness. However, MXene is predicted to possess larger electrical and heat conductivity than the corresponding MAX phase.[5,15] MXene has also been sought as a potential material for applications in electronic devices,[16–19] thermoelectric devices,[12,20] hydrogen storage,[21,22] gas sensors,[23] lead storage,[24] photo-catalysis,[25] optoelectronics[26] and electrochemical energy storage.[11,27–31]

Nb_4C_3[32] MXene, with one of the highest conductivity reported to date, has been synthesized recently from Nb_4AlC_3 using HF as an etchant. Like any other as-synthesized MXenes, the Nb_4C_3 layers were functionalized and Al atoms were also detected by X-ray photoemission spectroscopy.[5,33] Furthermore, structural distortions within the MXene layers were observed. The synthesized MXene had a C : Nb ratio differing from the ideal stoichiometry, which was attributed to the etching of Nb atoms by HF during the process of chemical exfoliation. Given its prospects in technology, the development of plausible isolation approaches to isolate pristine MXene layers, which are not terminated by Al or any functional group, from the MAX phase is highly desirable.

MXene has also been considered as a template to develop layered materials *via* controlled functionalization having tunable properties suitable for targeted applications. Several appealing theoretical predictions[12,21–23] were made by assuming the full coverage of MXene layers by the functional groups. Recent experimental studies,[34,35] revealing the uncontrolled, non-uniform and mixed functionalization of MXene layers, demonstrate serious challenges to the realization of its potential as predicted by

[a] *Materials Research Centre, Indian Institute of Science, Bangalore 560012, India. E-mail: abhishek@mrc.iisc.ernet.in*
[b] *Computational Science Research Center, Korea Institute of Science and Technology, Seoul, 02792, Republic of Korea*

† Electronic supplementary information (ESI) available. See DOI: 10.1039/c5cp07609a

‡ Contributed equally to this work.

Published on 22 March 2016. Downloaded by Korea Institute of Science and Technology / KIST on 29/07/2016 02:26:52.

theoretical studies. Therefore, synthesis of pristine MXene is essential not only for the unambiguous characterization of MXene, but also for the development of its derivatives by controlled functionalization, which are required for fabrication of devices with specific applications.

Using the first-principles calculations, we have investigated the atomistic mechanism of the transformation of MAX phase into pristine MXene *via* insertion of commonly used etchants – HF, alkali atoms and LiF – in Nb_4AlC_3 MAX phase. After the insertion, a search for the weaker bonds was carried out by calculating the bond-dissociation energies (BDE) for various bonds formed between the MXene layers of MAX phase. Rational explanation for the relative strengths of various bonds formed in a system is provided in detail using partial density of states and change transfer analysis. The HF insertion into MAX introduces huge anisotropy among the bond-dissociation energies of various bonds. However, compared to H–MXene the weak binding of H–F would lead to breaking of this bond and thereby ruling out the possibility of isolating pristine MXene. On the other hand the presence of Li in MAX weakens all the bonds between the MXene layers but due to competing BDE of alkali–MXene and alkali–Al, it does not facilitate the isolation of pristine MXene layers. The BDE for Li–MXene and F–Al bonds in Nb_4AlC_3 after LiF insertion is much smaller than that of other bonds formed between the MXene layers. However, a lower kinetic barrier for the dissociation of the Li–MXene bond compared to that of F–Al guarantees the dissociation of the Li–MXene bond under external perturbation. *Ab initio* molecular dynamics calculations clearly demonstrate the dissociation of the Li–MXene bond at 500 K leading to the isolation of a pristine MXene sheet, without any Al or functional group attached to it, from the MAX phase.

Methodology

First-principles calculations were performed using the Vienna *ab initio* simulation package (VASP).[36] Electron–ion interactions and electronic exchange correlations were approximated by all-electron projector augmented wave potentials (PAW)[37] and the Perdew–Burke–Ernzerhof (PBE)[38] generalized gradient approximation (GGA).[37,39] The plane-wave basis set with 500 eV cutoff was used. Brillouin zone sampling was done using a $6 \times 6 \times 1$ Monkhorst–Pack grid.[40] The density of states (DOS) calculations were done, using a denser $(15 \times 15 \times 1)$ k-grid. These parameters were tested to ensure the convergence of energy to less than 0.002 eV. The unit cell was optimized using the conjugate gradient scheme until the forces on every atom were <0.005 eV Å^{-1}. A large vacuum space (15 Å) was introduced in the simulation cell which was found sufficient to avoid any spurious cell–cell interaction. The lattice parameters obtained for Nb_4AlC_3 (a = 3.16 Å and c = 24.36 Å) were in good agreement with the experiments.[41] *Ab initio* molecular dynamics (AIMD) simulations were performed to access the dynamical properties of Nb_4AlC_3 with guest species with a time step of 1 fs within the canonical ensemble. The temperature was set at 500 K and adjusted *via* a Nosé-Hover thermostat.[42–44] For AIMD calculations, a 350 eV cut-off for the plane wave basis set was chosen. The calculations were performed on a unit cell, which contains 17 atoms (8 Nb, 6 C and one atom each of Al, Li and F). The effect of van der Waals forces on the binding of MXene layers appears to be very small and does not change our conclusions, except for increasing the absolute value of bond-dissociation energy ($\sim$0.3 eV) slightly. Therefore the results are presented here without including the van der Waals effects.

Results and discussion

Chemical exfoliation is extensively used to isolate the layers of graphene[45–49] and MoS_2.[3] In this process preliminary intercalation of guest species between the layers, often followed by sonication, facilitates the exfoliation of 2D-materials. Intercalating species expand the interlayer distance and significantly decrease the van der Waals binding between the layers. In contrast to graphite and MoS_2, the transformation of MAX phases to MXenes proceeds *via* chemical reactions, which can involve the insertion of reactants. A perusal of the MXene literature[9] clearly reveals that the Nb–C bond is much stronger than the Nb–Al bond. Using this fact, the insertion of guest atoms/molecules is carried out between the MXene layers with the aim to either break the Al–MXene bond or severely weaken it so that it can be broken easily.

A complete transformation of MAX to MXene consists of the isolation of one pristine MXene layer from the bulk without any Al or functional groups attached to it, while the other sheet remains covered with Al. The chemical transformation of Nb_4AlC_3 into Nb_4C_3 was studied using a model system, having vacuum–MXene–Al–MXene–vacuum geometry as shown in Fig. S1 (in ESI†). In order to determine the most stable position of an inserted guest atom/molecule, the formation energies corresponding to various configurations were calculated and defined as

$$E^{f} = E_{I\text{–}Nb_4AlC_3} - E_{Nb_4AlC_3} - \mu_I \quad (1)$$

where $E_{I\text{–}Nb_4AlC_3}$ and $E_{Nb_4AlC_3}$ are the energies of the MAX phase in the presence and absence of guest species, respectively. μ_I is the chemical potential of the guest species.

In MAX, the Nb atoms in both top and bottom MXene layers are bonded with the Al atom (Fig. S2a in ESI†) and, herein, will be referred as Nb_{top} and Nb_{bottom}. The inserted atom/molecule takes a position between Al and one MXene layer (here top) and, thus, increases the interlayer distance significantly and disrupts the bonding of Al with Nb_{top} (Fig. S2b–d in ESI†). However, the Al and Nb_{bottom} remained bonded. For the MAX with HF, E^{f} of the most favourable structure (Fig. S2b in ESI†) was found to be 0.57 eV where the μ_I was referenced to the total energy of the HF molecule. Here the H atom binds with Nb_{top} and F with Al, increasing the HF bond considerably. In Nb_4AlC_3 with Li (Fig. S2c in ESI†), for the most preferred position of the Li atom, the E^{f} was calculated to be 0.99 eV. μ_I was referenced to the total energy of the bulk bcc Li. The Li atom positions itself between Al and Nb_{top} and forms bonds with both Al and Nb_{top}.

 This journal is © the Owner Societies 2016

Published on 22 March 2016. Downloaded by Korea Institute of Science and Technology / KIST on 29/07/2016 02:26:52.

For Nb_4AlC_3 in the presence of LiF between MXene layers, the E^f for minimum energy structure (Fig. S2d in ESI†) was found to be −2.93 eV. The total energy of the bulk fcc LiF molecule was set as reference for μ_I. It indicates that the insertion of LiF in Nb_4AlC_3 is a favourable and spontaneous process. Here, Li and Al are attached to Nb_{top} and Nb_{bottom}, respectively, and F forms bonds with both Li and Al. The detailed structure of all the systems is given in ESI.†

Transformation of MAX to MXene involves breaking of bonds; therefore, the feasibility of transformation is measured by calculating the relative BDE for all the bonds formed between the MXene layers of Nb_4AlC_3 with the guest species. BDE is the amount of energy required to cleave a bond. BDE (ΔE) for a bond X–Y (where X/Y = Al, Nb, alkali, H, F) is calculated using the following equation:

$$\Delta E_{X-Y} = E_{d_c} - E_{d_e} \quad (2)$$

where E_{d_c} and E_{d_e} are the energies of the systems corresponding to the vertical distance between the X and Y atoms at d_c and d_e, respectively. d_e is the equilibrium vertical distance between X and Y atoms. Beyond d_c, the bond X–Y can be considered as a broken bond. BDE calculations are performed by fixing the lattice parameters and relaxing all the atoms in all the directions. The scheme used here to calculate BDE is demonstrated in Fig. S3 (ESI†). We first estimated the BDE for Al–MXene (Al–Nb) and Nb–C (Nb atom is bonded to Al) bonds in MAX phase, which are found to be 2.33 and 5.67 eV, respectively, as shown in Fig. 1a. Indeed, Nb–C bonds in MXene layers are quite strong. Generally, in 2D materials, weak van der Waals forces hold the 2D layers together. However, in MAX, the MXene layers are strongly bonded with each other *via* the Al–MXene bonds. Large BDE for Al–MXene bonds clearly indicates the challenges in exfoliating a pristine MXene from the MAX phase.

Next, we studied the insertion of various guest species and their effect on the BDE to check the possibility of isolation of pristine MXene. We first considered the effect of HF molecule insertion between the MXene layers of MAX phase. HF was recently employed as an etchant in the synthesis of Nb_4C_3; however, the atomistic details of the process are still not well understood. The BDE corresponding to the bonds H–$MXene_{top}$, Al–$MXene_{bottom}$, F–Al and F–H are 4.35, 2.22, 1.90 and 0.51 eV, respectively, as shown in Fig. 1b. Interestingly, the HF has introduced huge anisotropy in the BDE of various bonds in Nb_4AlC_3 with HF. Strong binding of H with MXene results in weakening of the H–F bond. Therefore, any external perturbation will break the H–F bond first, leaving functionalized MXene behind, in agreement with the experimental observations.[32] Hence, HF insertion would not transform MAX into pristine MXene.

We next studied the insertion of Li and other alkali atoms between MXene layers of the MAX phase. In contrast to the electronegative HF molecule (both H and F relative to Nb atoms) the alkali atoms are electropositive. As depicted in Fig. 1c, the BDE of Al–Nb_{bottom}, Li–Nb_{top} and Al–Li are 2.00, 0.89 and 0.79 eV, respectively. Although the presence of Li has weakened the Al–Nb_{bottom} bond, the Li–Al bond is weaker than the Al–Nb_{bottom} or Li–Nb_{top} bond. This clearly indicates that, when perturbed

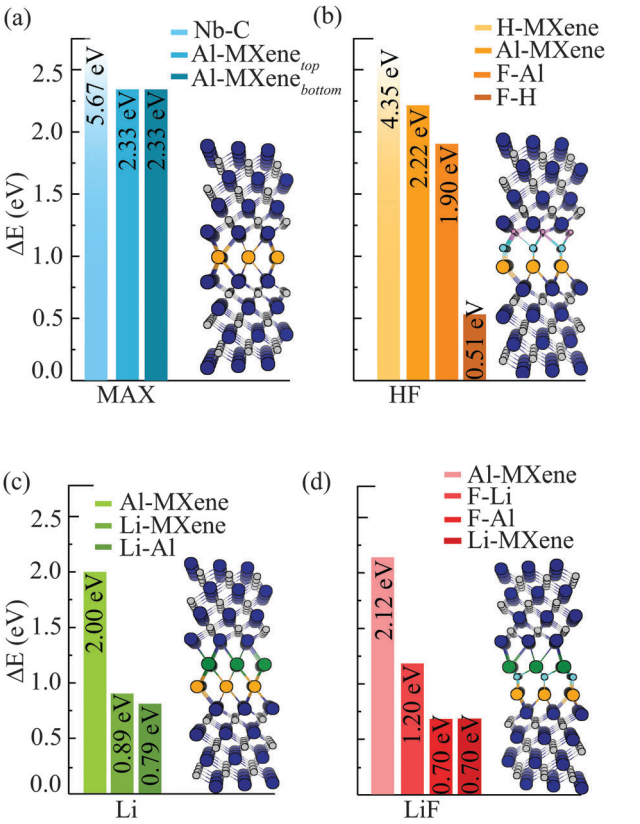

Fig. 1 (a) The structure and bond-dissociation energies of various bonds formed in Nb_4AlC_3. (b–d) Structure and bond-dissociation energies of various bonds formed in the presence of HF, Li, and LiF in Nb_4AlC_3, respectively. Nb, C, Al, Li, F, and H atoms are shown by blue, grey, orange, green, cyan, and pink balls, respectively.

externally, the Al–Li bonds readily break and result in the MXene layer that would have Li or Al attached to its surface. The possibility of isolating pristine MXene cannot be neglected as the BDE of the Li–Nb_{top} bond is only slightly higher (~0.14 eV) than that of Li–Al. Therefore, a small amount of pristine MXene may coexist with MXene with Li/Al attached to it, and hence, Li insertion cannot be employed for the isolation of pure pristine MXene. To assess the effect of size and ionization energy on the transformation of MAX, other alkali atoms, Na and K, were also investigated. Relaxed structures are very similar to Nb_4AlC_3 with Li, but with slightly different bond lengths (Table S1 in ESI†). With increasing size of the alkali atom the BDE of the alkali–MXene bond decreased (ΔE for Na/K is 0.80/0.79 eV), but the Al–alkali bond remained the weakest among all the bonds. Therefore, the insertion of electropositive alkali atoms into MAX cannot isolate pristine MXene.

BDE analysis of Nb_4AlC_3 with HF and Li clearly revealed the robust binding of H with MXene, whereas the binding of Nb with Li atoms was relatively weak. In comparison to Nb, the low ionization energy of Al resulted in strong binding of F with Al. Therefore, the insertion of LiF (F and Li atoms) in Nb_4AlC_3 was investigated in an attempt to weaken the MXene–LiF/Al bond. Structures with random orientation of Li–F (between the MXene layers of MAX phase) were also considered, but their energies

Published on 22 March 2016. Downloaded by Korea Institute of Science and Technology / KIST on 29/07/2016 02:26:52.

were considerably higher (<0.3 eV) than that of the structure shown in Fig. S2d (ESI†). Fig. 1d shows the BDE of various bonds in the lowest energy configuration of LiF in Nb_4AlC_3. The ΔE for Al–MXene, F–Al, F–Li and Li–MXene bonds are found to be 2.12, 0.70, 1.20 and 0.70 eV, respectively. As expected, the insertion of LiF molecules into MAX not only introduces anisotropy in the BDEs, but the bond formed between Li and MXene appears to be one of the weakest bonds. Similar BDEs for F–Al and Li–MXene bonds indicate that both the bonds can break with equal probability. Li–F dissociation leads to the isolation of pristine MXene from MAX. F–Al dissociation results in the formation of F–Li-terminated MXene and Al-terminated MXene. Interestingly, the BDE for FLi–MXene is only 0.02 eV. Since the lattice thermal energy at room temperature is ~25 meV, the spontaneous dissociation of FLi–MXene bonds can be achieved in experimental conditions. The dissociation of FLi–MXene bonds also leads to the isolation of pristine MXene.

Thermodynamics of the process has a major effect on the overall mechanism of the reaction; however, mostly the kinetics of the reaction control the isolation process. Therefore, we have calculated the energy barriers for the dissociation of F–Al and Li–MXene bonds in the MAX with LiF using the climbing image nudged elastic band (CI-NEB)[50,51] method. An interpolated chain of 8 different configurations (images) between the initial and final positions is taken. All the images are connected by springs and relaxed simultaneously to the minimum energy path (MEP). In the CI-NEB, the highest-energy image feels no spring force along the band and the direction of true force along the tangent is inverted. We used the same force tolerance for the barrier calculation as used for the structural relaxation. The energy barrier for the dissociation of F–Al and Li–MXene bonds was found to be 1.01 and 0.70 eV, respectively, as shown in Fig. S4 (ESI†). Contrary to the BDE calculations, the energy barrier for the dissociation of the F–Al bond is significantly higher than that of the Li–MXene bond. This clearly indicates that the isolation process will be dominated by the dissociation of Li–MXene bonds. Another interesting possibility emerges after the breaking of the F–Al bond, which leads to the formation of FLi–MXene and Al–MXene. The bond dissociation energy of FLi–MXene turns out to be 0.02 eV and this bond can break spontaneously at ambient temperature (300 K = 25 meV). Therefore, it provides us an alternative mechanism for separation of the pristine MXene sheet by LiF intercalation.

Indeed, BDE analysis provides a correct estimate of relative strengths of various bonds in the system. However, in order to gain a better insight into the relative bond strength, we next studied the atom-projected density of states (PDOS) of Nb_4AlC_3 systems. As the Nb–C bonds are much stronger than any other bond in this system, the PDOS analysis has been done for the atoms lying between the two MXene layers. The bond formation between Al and $Nb_{top/bottom}$ in MAX phase is prominently due to hybridization of Nb and Al states as clearly visible in Fig. 2a. The small splitting between bonding and anti-bonding states[52] of Al increases the stability of Al–Nb bonds. Upon HF insertion (Fig. 2b), interaction with HF significantly modifies the PDOS of Al. The H bonding states are located much below the

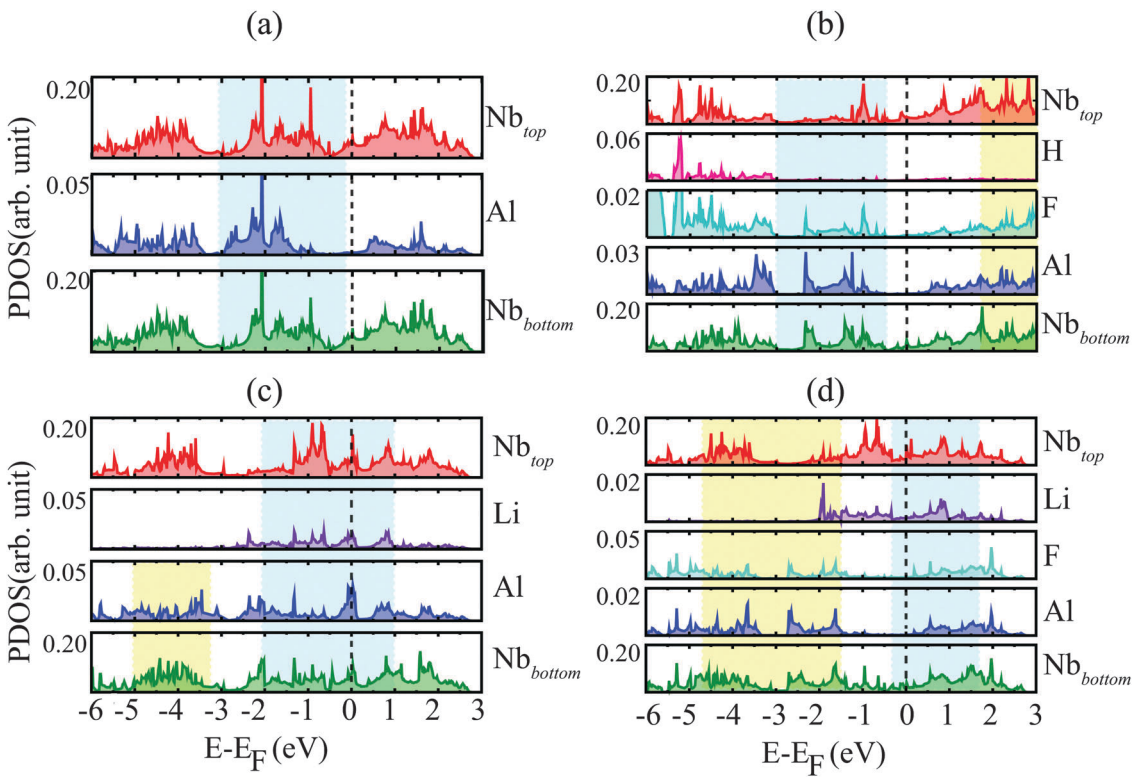

Fig. 2 Atom-projected DOS of (a) Nb_4AlC_3, and in the presence of (b) HF, (c) Li, and (d) LiF in Nb_4AlC_3.

 This journal is © the Owner Societies 2016

Published on 22 March 2016. Downloaded by Korea Institute of Science and Technology / KIST on 29/07/2016 02:26:52.

Fermi level. This is indicative of strong hybridization of H and Nb_{top} states, which results in a strong binding of H with MXene. Significant overlap of Al states with both Nb_{bottom} and F leads to stronger Al–MXene and Al–F bonds. The larger splitting between bonding and anti-bonding states of Al and F makes the Al–F bond stronger than the Al–MXene bond.

In the case of Nb_4AlC_3 with Li (Fig. 2c), all Al, Li, and Nb atoms have finite density of states diffused across the Fermi level, which indicates metallic bonding between Al–MXene, Al–Li and Li–MXene. Enhanced number of states at the Fermi level implies increased chemical activity leading to a weaker Al–MXene bond relative to that in MAX phase. Nevertheless, due to considerable overlap between Al and Nb_{bottom} states, the Al–Nb_{bottom} bond remains the strongest among all the bonds in the presence of Li in Nb_4AlC_3.

The PDOS of Nb_4AlC_3 in the presence of LiF are shown in Fig. 2d. Substantial overlap between F, Al and Nb_{bottom} states results in the stronger binding of Al with both F and MXene. Similar to the HF case, the splitting between bonding and anti-bonding states of F and Al will further strengthen the F–Al bond. Although Li atom states are diffused across the Fermi level, the overlap of Li states with the bonding states of F leads to a strong F–Li bond. As can be inferred from Fig. 2d, the presence of finite density of states of Li and Nb at the Fermi level renders the Li–MXene bond the most active/weak among all the bonds. PDOS analysis convincingly demonstrates the trend observed in BDE.

In order to examine the chemical nature of bonds (ionic, covalent, or metallic), we calculated the electron localization function (ELF). The ELF represents the probability of finding a pair of electrons at a given position.[53] The ELF values ranged between 0 and 1, where ELF = 1 corresponds to perfect localization (covalent bond), ELF = 0.5 corresponds to a homogeneous electron gas (metallic bond) and ELF = 0 corresponds to complete delocalization (no bond) between the atoms. The typical value of ELF for localized bonds is ≥ 0.75, and any value between 0.5 and 0.75 can be considered as metallic bonding. ELF contour plots are projected on the *XZ*-plane, passing through the Al atoms, as shown in Fig. 3a–d for Nb_4AlC_3. Fig. 3a shows the strong metallic bonding between Al and MXene layers in MAX phase; however, the electrons are more localized close to Al atoms. In the presence of HF in Nb_4AlC_3, the electrons are localized near F and H atoms, which reveals a strong ionic character of F–Al and H–MXene bonds (Fig. 3b). In the presence of Li in Nb_4AlC_3, a metallic bond forms between the Li–$MXene_{top}$ layers. Compared to MAX phase the binding of Al and $MXene_{bottom}$ has become weaker. The ELF analysis as shown in Fig. 3c indicates that, due to the presence of delocalized electrons (blue region) between Li and Al, the Li–Al bond is weaker than that formed between Li–$MXene_{top}$. In LiF inserted Nb_4AlC_3, the charge is more localized near the F atom demonstrating the ionic bonding between F–Al as shown in Fig. 3d and Fig. S5 (ESI†). Metallic bonding of Li with $MXene_{top}$ can also be inferred from Fig. 3d. The ELF analysis of Nb_4AlC_3 systems supports our conclusions regarding the relative strength of various bonds formed in these systems.

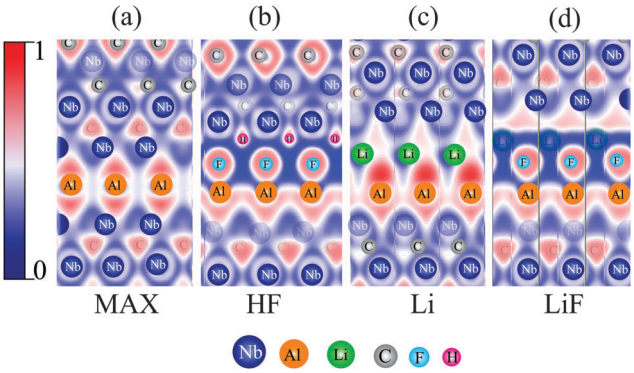

Fig. 3 Electron localization function (ELF) plots for (a) Nb_4AlC_3, and in the presence of (b) HF, (c) Li, and (d) LiF in Nb_4AlC_3.

The ELF analysis indicates the charge transfer between various atoms in the systems. The redistribution of states of Al and Nb atoms (Fig. 2a–d) also clearly demonstrates the strong charge transfer between the inserted species and, MXene and Al. To get a better quantitative insight, we estimates the charge transfer between various atoms by carrying out Bader charge analysis[54] as shown in Fig. 4a–d. As expected, the charge transfer between different atoms simply follows the trend of electronegativity of various atoms (F > C > H > Al > Nb > Li). For example, in Nb_4AlC_3, the more electronegative C and Al atoms attract the electron density away from the less electronegative Nb atoms (Fig. 4a). Upon insertion of HF in Nb_4AlC_3, Al and Nb_{top} atoms transfer charges to F and H, respectively, which results in the strong binding between Al–F and H–MXene. When Li is inserted into Nb_4AlC_3, as both Al and Nb are more electronegative, the Li atom loses its one electron to Al and Nb_{top} atoms. In Nb_4AlC_3 with LiF, significant charge transfer occurs from Al and Li to F. The presence of F between Al and Li reduces the direct charge transfer between them thereby reducing the binding of MXene with both Li and Al.

The analysis based on BDE convincingly shows the possibilities of transforming Nb_4AlC_3 into pristine MXene sheets upon

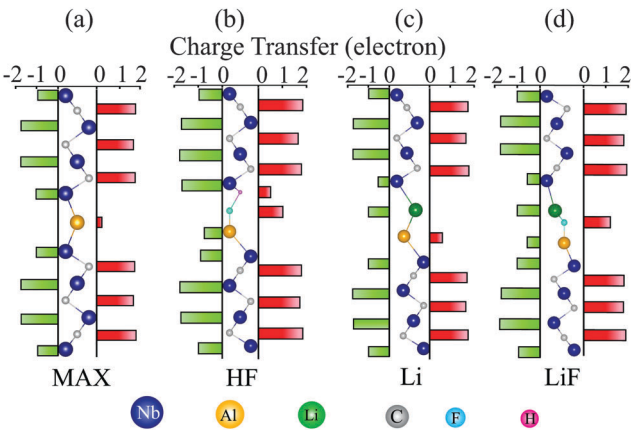

Fig. 4 Bader charge analysis for (a) Nb_4AlC_3, and in the presence of (b) HF, (c) Li, and (d) LiF in Nb_4AlC_3. Green and red color blocks show the charge transfer from or to the atoms.

Published on 22 March 2016. Downloaded by Korea Institute of Science and Technology / KIST on 29/07/2016 02:26:52.

insertion of LiF into MAX phase. We perform *ab initio* molecular dynamics calculations for the Nb_4AlC_3 systems with the inserted guest species, which can provide an unbiased microscopic insight into the dynamics of these systems at finite temperature. AIMD simulations were performed with the relaxed geometry and the real-time dynamics of the systems was monitored for 30 ps. In the presence of HF in Nb_4AlC_3, the weak bond between F and H was dissociated within 1 ps and the two layers (with one of them being H-functionalized MXene and other with Al–F attached to it) separated. After that the two layers remained separated with an interlayer distance of ~8.8 Å. No structural change or switching of functional groups was observed. The time evolution of isolation of MXene on HF insertion into Nb_4AlC_3 is shown in Fig. S6 (ESI†).

In the presence Li in Nb_4AlC_3, although static BDE calculations suggest that ΔE for the Al–Li bond is closer to that for F–H, the structural integrity (Fig. S2b in ESI†) was preserved till 800 K. Moreover, no bond dissociation was observed (Fig. S7 in ESI†). This indicates that the dissociation of these bonds involves larger kinetic barriers, which cannot be overcome till 800 K.

The thermal stability of Nb_4AlC_3 in the presence of LiF has been tested by a series of AIMD simulations, first using a $1 \times 1 \times 1$ cell, at different temperatures of 300, 400 and 500 K, and second with increased supercell size of $3 \times 3 \times 1$ (153 atoms) at 650 K. The $1 \times 1 \times 1$ cell structure was well maintained up to a temperature of 400 K. Upon increasing the temperature to 500 K, the Li–MXene bond was found to dissociate almost instantaneously, leading to the isolation of one pristine MXene sheet within 200 fs from the MAX phase, while the other sheet remained covered with Al. MD snapshots after 0.2 ps, 0.4 ps, 0.6 ps, 0.8 ps and 1 ps are shown in Fig. 5. Upon further continuation of the simulation, the Li–F layer also separated within 1 ps leaving the other MXene layer with Al attached to it. Once the pristine MXene separated out, within 3 ps, the distances between the pristine MXene, LiF and Al–MXene increased up to ~12 Å. We observed the dynamics for 30 ps, but the structure remained the same.

To further support our conclusions, we performed AIMD with $3 \times 3 \times 1$ supercell size at 500 K for ~20 ps. It is seen that the Nb–Li bond-length increases gradually; therefore to accelerate the process we increased the temperature to 650 K and within 3 ps the Nb–Li bonds dissociated completely (Nb–Li bond-length increased up to 20%) and led to the isolation of a pristine MXene sheet (Fig. 6). In sharp contrast to HF insertion, where MXene is always functionalized, AIMD results show that LiF insertion facilitates the isolation of a pristine MXene sheet. Furthermore, we performed metadynamics[55–57] simulations for MAX phase with LiF. The metadynamics simulation was performed using a $3 \times 3 \times 1$ supercell at a temperature of 600 K within the *NVT* ensemble. The length of Nb–Li bonds was defined as a collective variable. The average length of Nb–Li bonds increased gradually and in 2 ps 20% elongation of the bond was observed. The same elongation took place in AIMD simulations in 23 ps. Therefore, metadynamics simulations not only confirm the dissociation of the Li–MXene bond but also accelerate the simulation process.

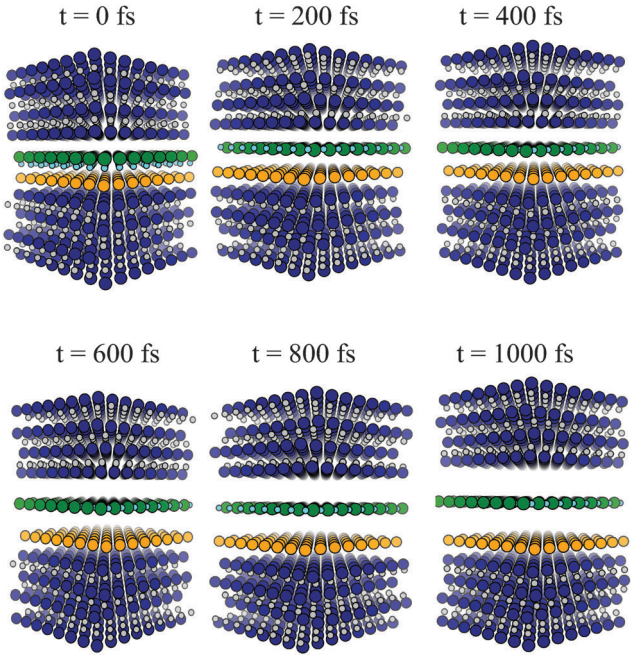

Fig. 5 Molecular dynamics snapshot in the presence of LiF in Nb_4AlC_3 at different time steps at 500 K.

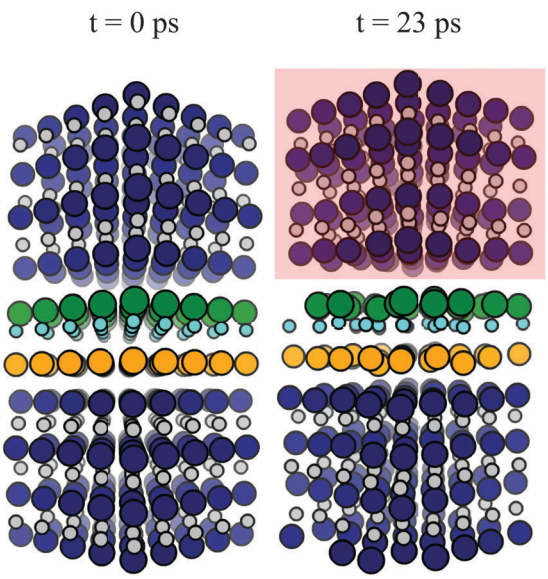

Fig. 6 Molecular dynamics snapshot in the presence of LiF in Nb_4AlC_3 with a $3 \times 3 \times 1$ supercell at initial and final time steps at 650 K.

Our results clearly demonstrate the feasibility of the isolation of pristine MXene after LiF insertion into MAX phase. Negative formation energy indicates that insertion of LiF into MAX phase is energetically favourable. Although similar to other 3D materials,[58–61] in experiments, the LiF can be inserted *via* edges or some other defects in the MAX phase, the process may involve some kinetic barrier. These calculations are computationally very demanding and beyond the scope of the present study. Therefore, our BDE results should be treated as a guideline for the experimentalist to find the appropriate guest molecules for exfoliation of pristine MXene.

 This journal is © the Owner Societies 2016

Published on 22 March 2016. Downloaded by Korea Institute of Science and Technology / KIST on 29/07/2016 02:26:52.

Our calculations also indicate that to transform the MAX phase into pristine MXene sheets, the guest species should have strong electronegative (*e.g.*, F) as well as electropositive (*e.g.* Alkali) elements. The electropositive element binds weakly with MXene, whereas F binds strongly with Al. The difference in the electronegativity of the elements in the inserted molecules is the key point for the transformation of MAX into pristine MXene. This is further demonstrated for the cases of NaF and KF in Nb_4AlC_3. Like LiF, NaF and KF insertion also leads to isolation of pristine MXene *via* strong anisotropy in BDE calculated by single point calculations as shown in Fig. S8 (ESI†), thereby facilitating the chemical transformation of MAX into pristine MXene under some external perturbation, *e.g.*, heating or sonication. At finite temperature, the barrier for the dissociation of bonds can be overcome. In sonication, the acoustic energy is dissipated as heat, which can help to overcome the barrier associated with the breaking of the weakest bond.

Conclusions

In conclusion, we have studied the chemical transformation of Nb_4AlC_3 MAX phase into Nb_4C_3 MXene upon insertion of HF, alkali atoms and LiF. By comparing the BDE of various bonds formed in the presence of HF, Li and LiF, we found that both HF and Li insertion into MAX did not facilitate the isolation of pristine MXene. Due to the strong binding of H and MXene, the HF insertion always results in functionalized MXene. The competitive bond strengths of Li–MXene and Li–Al in Li insertion blocked the possibility of transforming MAX into pristine MXene. In contrast, the insertion of LiF induces large anisotropy in the BDE of various bonds with the Li–MXene bond being one of the weakest among all the bonds. Furthermore, strong binding of F with both Li and Al ensures that in the presence of external perturbation, the weak Li–MXene bond breaks, leading to isolation of pristine MXene sheets. PDOS and ELF analyses provide insights into the relative strength and the chemical nature of various bonds. The different behavior of HF, Li and LiF has been explained in terms of charge transfer, which depends upon the relative electronegativities of the atoms. AIMD calculations at 500–650 K also show the isolation of pristine MXene from LiF insertion into Nb_4AlC_3. Our results not only give insights into the mechanism for isolation of MXene but also provide a general criterion for the selection of guest species which can be inserted for the transformation of MAX into pristine Nb_4C_3 layers in experiments.

Acknowledgements

We acknowledge the financial support of the Korea Institute of Science and Technology (Grant No. 2E25372). We also thank the Materials Research Centre and Supercomputer Education and Research Centre, Indian Institute of Science, and Institute of Materials Research (IMR) at Tohoku University, Japan for computing facilities. AKS and AM acknowledge the support from DST Nanomission.

References

1 K. S. Novoselov, A. K. Geim, S. V. Morozov, D. Jiang, Y. Zhang, S. V. Dubonos, I. V. Grigorieva and A. A. Firsov, *Science*, 2004, **306**, 666–669.
2 K. S. Novoselov, D. Jiang, F. Schedin, T. J. Booth, V. V. Khotkevich, S. V. Morozov and A. K. Geim, *Proc. Natl. Acad. Sci. U. S. A.*, 2005, **102**, 10451–10453.
3 J. N. Coleman, M. Lotya, A. O'Neill, S. D. Bergin, P. J. King, U. Khan, K. Young, A. Gaucher, S. De, R. J. Smith, I. V. Shvets, S. K. Arora, G. Stanton, H.-Y. Kim, K. Lee, G. T. Kim, G. S. Duesberg, T. Hallam, J. J. Boland, J. J. Wang, J. F. Donegan, J. C. Grunlan, G. Moriarty, A. Shmeliov, R. J. Nicholls, J. M. Perkins, E. M. Grieveson, K. Theuwissen, D. W. McComb, P. D. Nellist and V. Nicolosi, *Science*, 2011, **331**, 568–571.
4 J. R. Brent, N. Savjani, E. A. Lewis, S. J. Haigh, D. J. Lewis and P. O'Brien, *Chem. Commun.*, 2014, **50**, 13338–13341.
5 M. Naguib, M. Kurtoglu, V. Presser, J. Lu, J. Niu, M. Heon, L. Hultman, Y. Gogotsi and M. W. Barsoum, *Adv. Mater.*, 2011, **23**, 4248–4253.
6 I. R. Shein and A. L. Ivanovskii, *Micro Nano Lett.*, 2013, **8**, 59–62.
7 M. Naguib, O. Mashtalir, J. Carle, V. Presser, J. Lu, L. Hultman, Y. Gogotsi and M. W. Barsoum, *ACS Nano*, 2012, **6**, 1322–1331.
8 O. Mashtalir, M. Naguib, B. Dyatkin, Y. Gogotsi and M. W. Barsoum, *Mater. Chem. Phys.*, 2013, **139**, 147–152.
9 M. Naguib, V. N. Mochalin, M. W. Barsoum and Y. Gogotsi, *Adv. Mater.*, 2014, **26**, 992–1005.
10 A. N. Enyashin and A. L. Ivanovskii, *J. Phys. Chem. C*, 2013, **117**, 13637–13643.
11 Q. Tang, Z. Zhou and P. Shen, *J. Am. Chem. Soc.*, 2012, **134**, 16909–16916.
12 M. Khazaei, M. Arai, T. Sasaki, C.-Y. Chung, N. S. Venkataramanan, M. Estili, Y. Sakka and Y. Kawazoe, *Adv. Funct. Mater.*, 2013, **23**, 2185–2192.
13 M. Kurtoglu, M. Naguib, Y. Gogotsi and M. W. Barsoum, *MRS Commun.*, 2012, **2**, 133–137.
14 Y. Xie and P. R. C. Kent, *Phys. Rev. B: Condens. Matter Mater. Phys.*, 2013, **87**, 235441.
15 J. Halim, M. R. Lukatskaya, K. M. Cook, J. Lu, C. R. Smith, L.-Å. Näslund, S. J. May, L. Hultman, Y. Gogotsi, P. Eklund and M. W. Barsoum, *Chem. Mater.*, 2014, **26**, 2374–2381.
16 H. Zhao, C. Zhang, S. Li, W. Ji and P. Wang, *J. Appl. Phys.*, 2015, **117**, 085306.
17 Y. Lee, Y. Hwang and Y.-C. Chung, *ACS Appl. Mater. Interfaces*, 2015, **7**, 7163–7169.
18 X. Li, Y. Dai, Y. Ma, Q. Liu and B. Huang, *Nanotechnology*, 2015, **26**, 135703.
19 L.-Y. Gan, Y.-J. Zhao, D. Huang and U. Schwingenschlögl, *Phys. Rev. B: Condens. Matter Mater. Phys.*, 2013, **87**, 245307.
20 M. Khazaei, M. Arai, T. Sasaki, M. Estili and Y. Sakka, *Phys. Chem. Chem. Phys.*, 2014, **16**, 7841–7849.
21 Q. Hu, D. Sun, Q. Wu, H. Wang, L. Wang, B. Liu, A. Zhou and J. He, *J. Phys. Chem. A*, 2013, **117**, 14253–14260.
22 Q. Hu, H. Wang, Q. Wu, X. Ye, A. Zhou, D. Sun, L. Wang, B. Liu and J. He, *Int. J. Hydrogen Energy*, 2014, **39**, 10606–10612.

Published on 22 March 2016. Downloaded by Korea Institute of Science and Technology / KIST on 29/07/2016 02:26:52.

23 X.-f. Yu, Y.-c. Li, J.-b. Cheng, Z.-b. Liu, Q.-z. Li, W.-z. Li, X. Yang and B. Xiao, *ACS Appl. Mater. Interfaces*, 2015, **7**, 13707–13713.
24 Q. Peng, J. Guo, Q. Zhang, J. Xiang, B. Liu, A. Zhou, R. Liu and Y. Tian, *J. Am. Chem. Soc.*, 2014, **136**, 4113–4116.
25 O. Mashtalir, K. Cook, V. Mochalin, M. Crowe, M. Barsoum and Y. Gogotsi, *J. Mater. Chem. A*, 2014, **2**, 14334–14338.
26 H. Lashgari, M. Abolhassani, A. Boochani, S. Elahi and J. Khodadadi, *Solid State Commun.*, 2014, **195**, 61–69.
27 M. Naguib, J. Halim, J. Lu, K. M. Cook, L. Hultman, Y. Gogotsi and M. W. Barsoum, *J. Am. Chem. Soc.*, 2013, **135**, 15966–15969.
28 D. Er, J. Li, M. Naguib, Y. Gogotsi and V. B. Shenoy, *ACS Appl. Mater. Interfaces*, 2014, **6**, 11173–11179.
29 Z. Ling, C. E. Ren, M.-Q. Zhao, J. Yang, J. M. Giammarco, J. Qiu, M. W. Barsoum and Y. Gogotsi, *Proc. Natl. Acad. Sci. U. S. A.*, 2014, **111**, 16676–16681.
30 M. R. Lukatskaya, O. Mashtalir, C. E. Ren, Y. Dall'Agnese, P. Rozier, P. L. Taberna, M. Naguib, P. Simon, M. W. Barsoum and Y. Gogotsi, *Science*, 2013, **341**, 1502–1505.
31 Y. Xie, Y. Dall'Agnese, M. Naguib, Y. Gogotsi, M. W. Barsoum, H. L. Zhuang and P. R. C. Kent, *ACS Nano*, 2014, **8**, 9606–9615.
32 M. Ghidiu, M. Naguib, C. Shi, O. Mashtalir, L. M. Pan, B. Zhang, J. Yang, Y. Gogotsi, S. J. L. Billinge and M. W. Barsoum, *Chem. Commun.*, 2014, **50**, 9517–9520.
33 O. Mashtalir, M. Naguib, V. N. Mochalin, Y. Dall'Agnese, M. Heon, M. W. Barsoum and Y. Gogotsi, *Nat. Commun.*, 2013, **4**, 1716.
34 L. H. Karlsson, J. Birch, J. Halim, M. W. Barsoum and P. O. Å. Persson, *Nano Lett.*, 2015, **15**, 4955–4960.
35 X. Wang, X. Shen, Y. Gao, Z. Wang, R. Yu and L. Chen, *J. Am. Chem. Soc.*, 2015, **137**, 2715–2721.
36 P. E. Blöchl, *Phys. Rev. B: Condens. Matter Mater. Phys.*, 1994, **50**, 17953–17979.
37 G. Kresse and D. Joubert, *Phys. Rev. B: Condens. Matter Mater. Phys.*, 1999, **59**, 1758–1775.
38 J. P. Perdew, K. Burke and M. Ernzerhof, *Phys. Rev. Lett.*, 1997, **78**, 1396.
39 G. Kresse and J. Furthmüller, *Comput. Mater. Sci.*, 1996, **6**, 15–50.
40 H. J. Monkhorst and J. D. Pack, *Phys. Rev. B: Solid State*, 1976, **13**, 5188–5192.
41 C. Hu, F. Li, J. Zhang, J. Wang, J. Wang and Y. Zhou, *Scr. Mater.*, 2007, **57**, 893–896.
42 S. Nosé, *J. Chem. Phys.*, 1984, **81**, 511–519.
43 W. G. Hoover, *Phys. Rev. A: At., Mol., Opt. Phys.*, 1985, **31**, 1695–1697.
44 N. Shuichi, *Prog. Theor. Phys. Suppl.*, 1991, **103**, 1–46.
45 M. Segal, *Nat. Nanotechnol.*, 2009, **4**, 612–614.
46 S. Stankovich, D. A. Dikin, R. D. Piner, K. A. Kohlhaas, A. Kleinhammes, Y. Jia, Y. Wu, S. T. Nguyen and R. S. Ruoff, *Carbon*, 2007, **45**, 1558–1565.
47 G. Eda, G. Fanchini and M. Chhowalla, *Nat. Nanotechnol.*, 2008, **3**, 270–274.
48 X. Li, G. Zhang, X. Bai, X. Sun, X. Wang, E. Wang and H. Dai, *Nat. Nanotechnol.*, 2008, **3**, 538–542.
49 P. K. Ang, S. Wang, Q. Bao, J. T. Thong and K. P. Loh, *ACS Nano*, 2009, **3**, 3587–3594.
50 G. Henkelman, B. P. Uberuaga and H. Jónsson, *J. Chem. Phys.*, 2000, **113**, 9901–9904.
51 G. Henkelman and H. Jónsson, *J. Chem. Phys.*, 2000, **113**, 9978–9985.
52 R. Hoffmann, *Angew. Chem., Int. Ed.*, 1987, **26**, 846–878.
53 B. Silvi and A. Savin, *Nature*, 1994, **371**, 683–686.
54 W. Tang, E. Sanville and G. Henkelman, *J. Phys.: Condens. Matter*, 2009, **21**, 084204.
55 A. Laio and M. Parrinello, *Proc. Natl. Acad. Sci. U. S. A.*, 2002, **99**, 12562–12566.
56 M. Iannuzzi, A. Laio and M. Parrinello, *Phys. Rev. Lett.*, 2003, **90**, 238302.
57 B. Ensing, A. Laio, M. Parrinello and M. L. Klein, *J. Phys. Chem. B*, 2005, **109**, 6676–6687.
58 C. Xia, S. Watcharinyanon, A. A. Zakharov, R. Yakimova, L. Hultman, L. I. Johansson and C. Virojanadara, *Phys. Rev. B: Condens. Matter Mater. Phys.*, 2012, **85**, 045418.
59 M. Z. Bazant, *Acc. Chem. Res.*, 2013, **46**, 1144–1160.
60 E. Uchaker, H. Jin, P. Yi and G. Cao, *Chem. Mater.*, 2015, **27**, 7082–7090.
61 L. Wei, F. Wu, D. Shi, C. Hu, X. Li, W. Yuan, J. Wang, J. Zhao, H. Geng, H. Wei, Y. Wang, N. Hu and Y. Zhang, *Sci. Rep.*, 2013, **3**, 2636.

 This journal is © the Owner Societies 2016